Pichler, Thomas ; Ridley, W.Ian ; Nelson, Eric

Low-temperature alteration of dredged volcanics from the Southern Chile Ridge: additional information about early stages of seafloor weathering

Journal Article as: peer-reviewed accepted version (Postprint)

DOI of this document*(secondary publication): https://doi.org/10.26092/elib/3254

Publication date of this document: 26/08/2024

* for better findability or for reliable citation

Recommended Citation (primary publication/Version of Record) incl. DOI:

Thomas Pichler, W.Ian Ridley, Eric Nelson, Low-temperature alteration of dredged volcanics from the Southern Chile Ridge: additional information about early stages of seafloor weathering, Marine Geology, Volume 159, Issues 1–4, 1999, Pages 155-177, ISSN 0025-3227, https://doi.org/10.1016/S0025-3227(99)00008-0.

Low-temperature alteration of dredged volcanics from the Southern Chile Ridge: additional information about early stages of seafloor weathering

Thomas Pichler [a,*], W. Ian Ridley [b], Eric Nelson [c]

[a] *Department of Geology, University of Ottawa, Ottawa-Carleton Geoscience Center, PO Box 450, Stn. A, Ottawa, Ontario, Canada K1N 6N5*

[b] *Branch of Geochemistry, U.S. Geological Survey, Denver, CO 80225, USA*

[c] *Department of Geology and Geological Engineering, Colorado School of Mines, Golden, CO 80401, USA*

[*] Corresponding author. Tel.: +1-613-562-5800, ext. 6639; Fax: +1-613-562-5192; E-mail: tpichler@nrcan.gc.ca

1. Introduction

The process of submarine weathering, i.e., low temperature alteration under near-to-ambient conditions, is characterized by several stages of alteration which are controlled by different water±rock ratios, oxidation coefficients, direction of element exchange, water content and isotopic changes (Honnorez, 1981; Thompson, 1991). Hart (1970) quantified low temperature alteration into four stages: (1) unaltered with H_2O content lower than 0.3% and Fe^{3+}/Fe^{2+} from 0.2 to 0.3; (2) `partially altered' $H_2O$ ranging from 0.4 to 0.7%; (3) altered with $H_2O$ content ranging from 0.6 to 1%, $Fe^{3+}/Fe^{2+} > 0.3$ and an increase in Cs, Rb and K; (4) `highly altered' H_2O content larger than 1%. This classification, however, is based solely on chemical attributes without considering mineralogical aspects. A difficulty with a purely chemical classification arises once alteration proceeds to stages 3 and 4 and chemical analyses need to be normalized to overcome the problem of misleading element mobility due to volume change (Gresens, 1967; Grant, 1986). The initial texture, mineral composition and glassy fraction are likely to be crucial factors controlling alteration.

We acquired a suite of rocks from the Southern Chile Ridge showing degrees of alteration from stage 1 to stage 3 on the Hart and Nalwalk scale. This range of alteration can be observed between samples and between alteration halos of individual samples, enabling a detailed mineralogical and chemical study of the initial stages of low temperature alteration.

2. Location and tectonic setting of study area

The study area is located along the Southern Chile Ridge (SCR) NW of the Taitao Peninsula and extends from approximately 46°S and 76°W to approximately 43°S and 82°W. Dredge samples were collected during the southern CROSS expedition in 1993. The Chile Ridge-Trench triple junction, located at approximately 46°S, marks the juncture

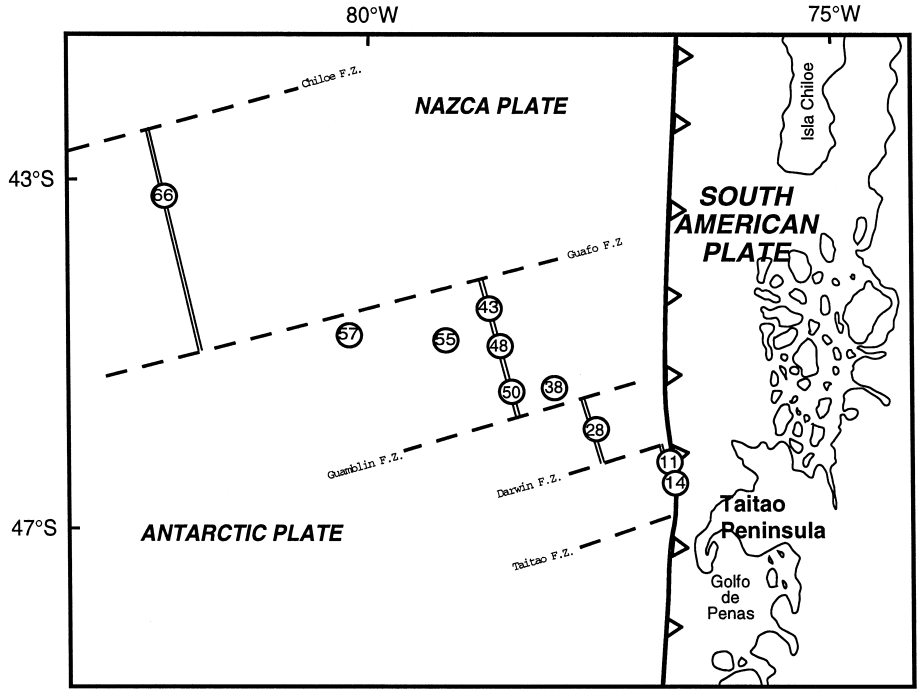

Fig. 1. Tectonic setting and locations of dredge stations along the Southern Chile Ridge and at off-axis seamounts where altered rocks were recovered.

between the Nazca, Antarctic and South American plates (Fig. 1) where the Chile Ridge is being consumed beneath the South American plate (Cande and Leslie, 1986; Nelson and Forsythe, 1989).

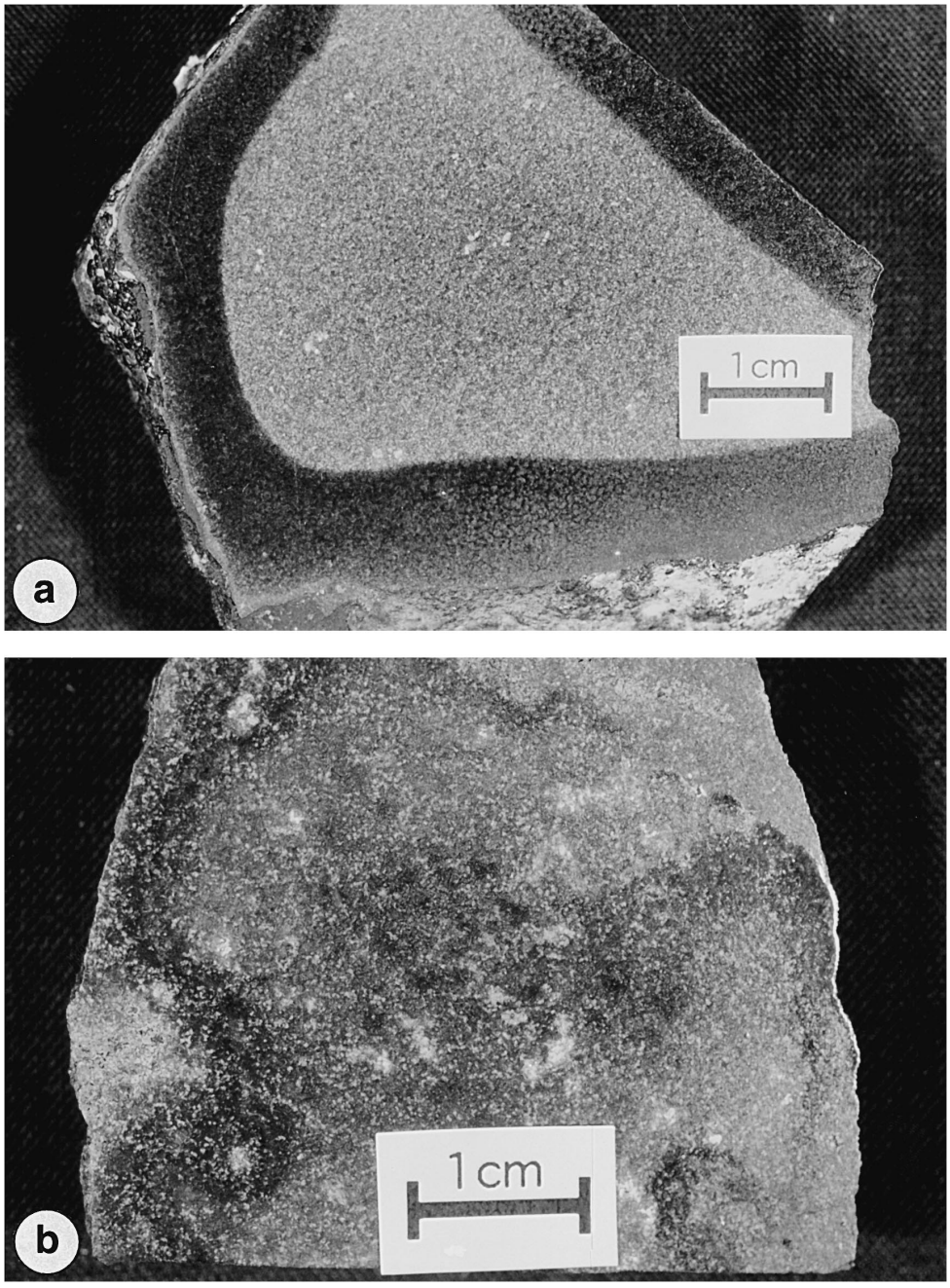

Fig. 2. Photographs of polished rock slabs from sample 38a. (a) Sample with distinct alteration zones. The darker outer zones contains mainly a mixture of celadonite and Fe-oxyhydroxide. In the lighter interior saponite is the major secondary alteration phase. (b) Pervasively altered sample. Lighter areas are due to the presence of secondary Fe-oxyhydroxide and celadonite/Fe-oxyhydroxide.

3. Analytical methods

Sixteen (16) samples (Appendix A) from 10 dredge sites were selected for study after macroscopic examination of sawed surfaces of which 11 were selected for further geochemical analyses following thin section examination. The protoliths of most samples were basaltic pillows, based upon (a) they have angular outlines due to breakage along cooling cracks, (b) they show alteration halos or discontinuous zones parallel to crack surfaces or the original pillow surface and (c) increasing size of vesicles towards the original pillow surface. If well developed, the zones were designated A > B > C > D, etc., in inward succession. For example, `B, 1.5±2.5 cm, brown', describes the second zone, colored brown, located between 1.5±2.5 cm inward from the surface (Appendix A). Examination of macroscopic alteration features, e.g., color differences (Fig. 2a) from gray (freshest) to brown (most altered), and occurrence of alteration halos and Mn-crusts, indicated that the relative degree of alteration progresses in the sample order: 66-9 < 48-1 < 50-5 < 38a < 57-5 < 38d < 57-7 < 38b < 57-2.

A definite identification of secondary mineral phases was usually obtained through a combination of thin section petrography, XRD and electron microprobe analysis. Alteration halos that were too small to be separated with a rock saw were drilled with a dental drill and collected as powders.

3.1. XRD methods

Powdered rock samples were mounted in a round aluminum holder using the backloading technique (Moore and Reynolds, 1989). They were scanned continuously from 4.00° to 45.00° 2θ using copper X-radiation generated at 30 kV and 15 mA. Air dried and ethylene glycol-solvated clay-size fractions (Moore and Reynolds, 1989) were scanned from 2.00° to 55.00° 2θ stepping 0.2° 2θ using copper X-radiation generated at 35 kV and 15 mA. Primary and secondary minerals identified by XRD are shown in Table 1.

3.2. Electron microprobe methods

Analyses of phases in carbon-coated polished thin sections were performed on a automated JEOL Superprobe JXA-8900L using 15 kV accelerating voltage, 2 nA beam current and beam diameters varying from < 1 mm to 5 mm. Data were reduced using a ZAF correction procedure. The quality of the data was estimated from structural formulae calculated from chemical analyses. Analyses were accepted if the structural formula was stoichiometric ($\pm$0.2 units for the octahedral total for saponite) and oxyhydroxide totals were higher than 74%.

3.3. Major, minor and trace element methods

Na, Mg, Al, Si, P, K, Ti, Mn and Fe were analyzed by wavelength-dispersive X-ray fluorescence spectroscopy (WD-XRF) using a Phillips PW1600 X-ray spectrometer. Analytical error is less than ~1% for Si, Mg, Fe, Al, Ca and less than 3% for P, K, Ti, Mn, Na (Taggart et al., 1987). Fe is reported as Fe^{3+}. Fe^{2+} was determined by potentio-

Table 1
X-ray diffraction results for scans of whole rock powders and clay size separates

Sample	Whole rock scan	Clay separate (air dried)	Clay separate (glycolated)
38a	Anorthite (intermediate), augite, forsterite	dehydrated smectite (12 Å)	Smectite (17 Å)
38b	Anorthite (intermediate), augite	Illite/celadonite?	no distinct peaks
38d	Anorthite (intermediate), augite	no distinct peaks	no distinct peaks
48-1	no scan	no distinct peaks	no distinct peaks
50-5	Anorthite (intermediate), augite	Smectite (14.5 Å)	Smectite (17 Å)
57-2	Anorthite (intermediate), augite	dehydrated smectite (12.5 Å)	Smectite (17 Å)
57-5	Anorthite (intermediate), augite, forsterite	no distinct peaks	no distinct peaks
57-7	Anorthite (intermediate), augite	Smectite (14.4 Å)	Smectite (17 Å)
66-9	Anorthite (intermediate), augite, forsterite	Smectite (14.6 Å)	Smectite (17 Å)

Notes: Clay separates were scanned air dried and after glycolation with ethylene glycol for 24 h.

metric titration (USGS, Open File Report 90.668, p. 139).

Rare earth elements (REE), Rb, Sr, Y, Zr, Nb, Mo, Cs, Ba, Hf and Ta were analyzed from fused powders by laser microprobe using a VG PQ2 + Plasma Quad ICP-MS with a Laserlab laser ablation system. The system setup, calibration and sample preparation procedures were adapted from Perkins et al. (1993).The analytical error for the above described method is better than 15% (Perkins et al., 1993).

3.4. Water method

Total water content was analyzed by Karl Fisher titration for H_2O^+ (essential water) and weight loss following heating of the sample for H_2O^- (moisture) following Norton and Papp (1990). The accuracy of this method has been determined and the recommended analytical error is $\sim$1.5% (Norton and Papp, 1990).

4. Results

4.1. Mineralogy

Concentric alteration halos can be recognized in hand samples by distinct or subtle color changes (Fig. 2a). However, some samples were pervasively altered (Fig. 2b). The fresh protoliths of most samples (Appendix A) were probably basaltic pillow lava with glomeroporhyritic, spherulitic and variolitic textures and a glassy to microcrystalline matrix. Plagioclase was the most abundant primary mineral followed by olivine and clinopyroxene.

Typical alteration features include crack and/or vesicle fillings, replacement of groundmass and olivine crystals with yellowish secondary mineral phases and oxidation of magnetite. Alteration zones are recognized microscopically by the intensity of vesicle/crack filling and degree of replacement of glassy matrix with secondary mineral phases. Secondary minerals identified include celadonite (dioctahedral mica with the general formula $K[Mg,Fe^{2+}][Fe^{3+},Al]Si_4O_{10}[OH]_2$), saponite (trioctahedral smectite with the general formula $X[Mg,Fe^{2+},Fe^{3+}]_3[Si,Al]_4O_{10}[OH]_2 4H_2O$, where X = interlayer Na, Ca), Fe-oxyhydroxide (FeOOH polymorphs, including goethite), and hematite. Proceeding outwards from a fracture into the massive rock displays a discrete zonation of secondary minerals in the order Fe-oxyhydroxide followed by celadonite/Fe-oxyhydroxide and finally saponite. However, there are exceptions to this order, such as (1) saponite may rim (Fig. 3a) or be rimmed by a mixture of celadonite and Fe-oxyhydroxide (Fig. 3b), and (2) vesicles may be filled by red-colored Fe-

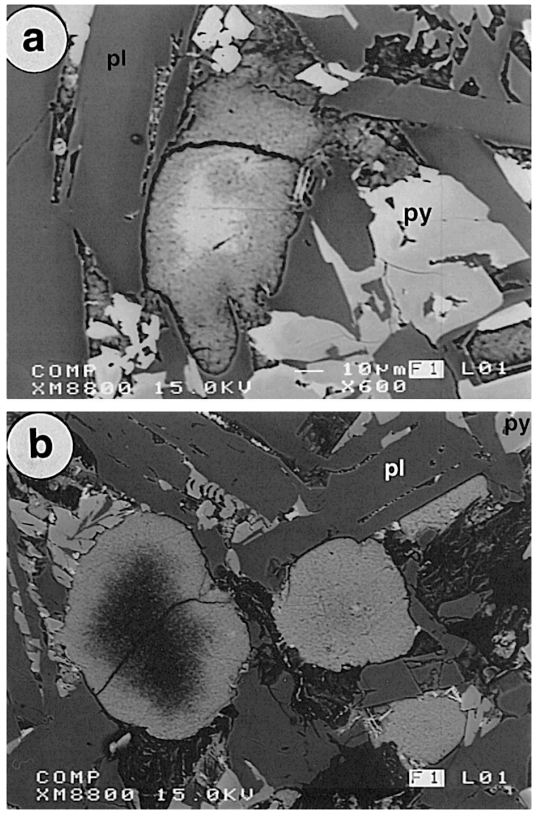

Fig. 3. Backscatter images. (a) Sample 38a. Saponite, transition mineral and celadonite/Fe-oxyhydroxide replacing a primary mineral phase (olivine?). Celadonite/Fe-oxyhydroxide is located in the center (bright color) and rimmed by transition mineral and saponite (darker color). The dark elongated crystals on the left side and upper right side are plagioclase (pl). The bright colored crystals on the lower right side are pyroxene (py). (b) Sample 57-2. Saponite and celadonite/Fe-oxyhydroxide replacing a primary mineral phase (olivine?). Saponite (dark color) is located in the center and rimmed by celadonite/Fe-oxyhydroxide (bright color). To the right celadonite/Fe-oxyhydroxide replaces intersertal groundmass. The dark elongated crystals are plagioclase (pl).

oxyhydroxide (possibly goethite) rimmed by a yellow-colored mixture of celadonite/Fe-oxyhydroxide.

Structural formulae for secondary clay minerals were calculated on the basis of $O_{10}(OH)_2$ following the procedure adopted by Ross and Hendricks (1945). Si^{4+}, Al^{3+}, and Fe^{3+} were assigned to the tetrahedral layer, in that order, to provide a total of four cations. Ti^{4+}, Mg^{2+}, Mn^{2+} and Fe^{2+}, together with excess Fe^{3+} and Al^{3+}, when present, were assigned to the octahedral layer. Ca^{2+}, K^{+} and Na^{+} were apportioned to the interlayer sites. Octahedral totals were calculated for celadonite/Fe-oxyhydroxides using the same procedure.

4.1.1. Saponite

Colorless, yellow, brown, and red varieties of saponite replace microcrystalline groundmass, glass and olivine. Ca is the dominant interlayer cation in brown and red saponite whereas K is the dominant interlayer cation in colorless and yellow varieties. Fe/(Fe + Mg) values range from 0.1 to 0.5 (Table 2

Table 2
Representative microprobe analyses of secondary minerals in altered rock samples from the Southern Chile Ridge

Sample:	57-5 1b	38a-6e	38d-3b	38a-2b	57-2-2d	57-2-3c
Mineral:	Fe-oxyhydroxide	Celadonite/	Celadonite/	Transition mineral	Saponite	Saponite
Color:	Red	Fe-oxyhydroxide	Fe-oxyhydroxide	Red brown	Yellow white	Brown
Occurrence:	Groundmass	Yellowish brown Vesicle	Light yellow Groundmass	Groundmass	Groundmass	Groundmass
SiO_2	5.82	46.14	47.30	43.25	48.87	46.52
Al_2O_3	2.13	0.93	4.32	0.14	3.09	4.92
MgO	2.38	4.34	4.02	7.24	13.79	18.97
FeO^T	69.41	31.82	27.14	33.83	14.45	5.05
MnO	2.08	0.06	0.00	0.07	0.00	0.06
CaO	0.50	0.91	0.63	1.14	0.28	1.47
Na_2O	0.10	0.11	0.17	0.20	0.32	0.13
K_2O	0.09	4.96	5.97	2.09	2.09	0.19
TiO_2	0.00	0.03	0.09	0.00	0.03	0.04
Total	82.50	89.29	89.63	87.96	82.92	77.35
Calculated Formula (Atoms)						
Tetrahedral						
Si	0.806	3.864	3.834	3.699	3.900	3.758
Al	0.347	0.092	0.166	0.014	0.100	0.242
Fe	2.848	0.044	0.000	0.287	0.000	0.000
Octahedral						
Al	0.000	0.000	0.247	0.000	0.191	0.227
Mg	0.492	0.541	0.486	0.923	1.641	2.284
Fe^{2+}/Fe^{3+}	5.191	2.186	1.840	2.132	0.965	0.341
Mn	0.244	0.004	0.000	0.005	0.000	0.004
Ti	0.000	0.002	0.005	0.000	0.002	0.003
Octahedral total	5.926	2.733	2.578	3.060	2.798	2.858
Interlayer						
Ca	0.073	0.081	0.054	0.105	0.024	0.127
Na	0.028	0.018	0.027	0.033	0.049	0.020
K	0.015	0.530	0.617	0.228	0.213	0.020
Interlayer total	0.116	0.629	0.698	0.365	0.286	0.167
Total	10.043	7.362	7.276	7.425	7.084	7.025
Al total	0.347	0.092	0.413	0.014	0.291	0.469
Fe total	8.039	2.230	1.840	2.419	0.965	0.341
Fe/Fe + Mg	0.942	0.805	0.791	0.724	0.370	0.130

Notes: Structural formulas were calculated on the basis of $O_{10}(OH)_2$. Fe is assumed to be Fe^{2+} in saponite and Fe^{3+} in celadonite/Fe-oxyhydroxide.

and Fig. 4). Al contents are generally less than 0.5 atoms per formula unit.

4.1.2. Celadonite / Fe-oxyhydroxide

Celadonite/Fe-oxyhydroxide mixtures that were identified by microprobe analyses are the most abundant alteration products, and based on visual observation, most samples contained more than 5%. Analyses are shown in Table 2. When cation proportions are plotted vs. interlayer K (Fig. 4) many of the celadonite/Fe-oxyhydroxides analyzed fall into the celadonite field. Generally, however, celadonite/Fe-oxyhydroxides have lower K, higher Fe values, and higher octahedral totals than celadonite. Structural formulae are not consistent with a di-octahedral mineral, thus we have interpreted the chemical compositions as a mixture of celadonite and Fe-oxyhydroxide. K_2O and FeO^T are correlated with color. Pale yellow celadonite/Fe-oxyhydroxides have lower FeO^T values ($\sim$25 wt.%) and higher K_2O ($\sim$6 wt.%) than pale brown celadonite/Fe-oxyhydroxides (36 wt.%, 3 wt.%). Vesicles filled with celadonite/Fe-oxyhydroxide may be compositionally zoned from early pale yellow to later pale brown types (Table 2).

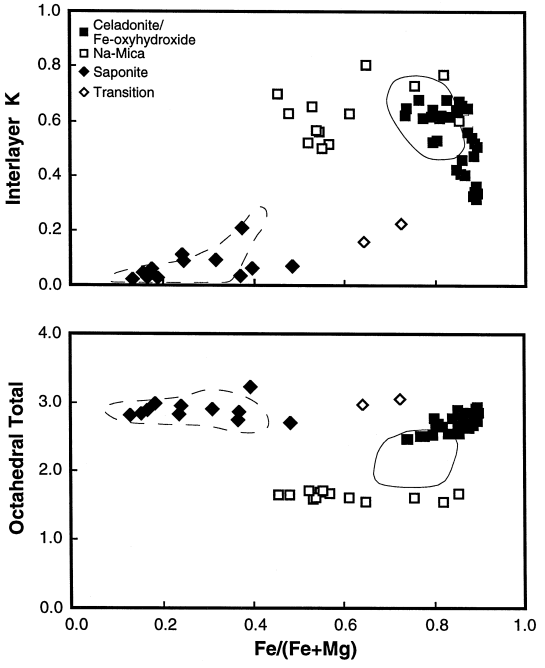

Fig. 4. Number of K atoms in the interlayer (a) and number of octahedral atoms (b) plotted vs. Fe/(Fe+Mg). Calculations of structural compositions were made from microprobe analyses on the basis of $O_{10}(OH)_2$. Fields for saponite (dashed line) and celadonite (solid line) are from Pichler (1994).

4.1.3. Fe-oxyhydroxides

Secondary Fe-oxyhydroxides are observed immediately adjacent to cracks and/or close to the sample surface. Single crystal XRD analyses reveal goethite and hematite as the major phases with minor amounts of iwakiite. Their bright red color and optical isotropy distinguishes them from celadonite/Fe-oxyhydroxide. Fe-oxyhydroxide mainly fills vesicles and small discontinuous cracks. Fe-oxyhydroxides have lower K_2O and higher FeO concentrations than celadonite/Fe-oxyhydroxide (Table 2). The detection of SiO_2 is consistent with other Fe-oxyhydroxides analyzed in altered submarine basalt (Honnorez, 1981; Alt, 1993).

4.1.4. Transition phase

A secondary material, present in rare samples, e.g., 38a (Fig. 3b), has a transitional composition between saponite and celadonite/Fe-oxyhydroxide. Fe/(Fe + Mg) values are too high for celadonite, and K_2O values are too low to for celadonite/Fe-oxyhydroxide (Fig. 4). The calculated structural formula is that of an Fe-rich tri-octahedral smectite. Given the small amounts present, microprobe analyses was our only means to investigate this material. It may well be only a physical mixture of celadonite and saponite if individual particles are smaller than the diameter of the electron beam.

4.2. Rock chemistry

The results of major, minor, trace and rare earth element analyses are listed in Appendices B and C. The principal reaction between seafloor rocks and seawater at low temperature is hydration of primary minerals and precipitation of hydrous secondary minerals. Thus, the H_2O content of seafloor rocks can be used as a sensitive indicator of their magnitude of alteration (Hart, 1969; Alt et al., 1992; Alt, 1993). To eliminate dilution effects due to volume changes (Gresens, 1967) chemical analyses were recalculated on a water free basis (Honnorez, 1981)

before being displayed graphically. SiO_2, $Fe_2O_3^T$, MgO, MnO, CaO and K_2O are plotted vs. H_2O for samples with distinct alteration halos in Fig. 5. Relative to the freshest parts of each rock, and as a function of H_2O content: (1) CaO consistently decreases with increasing H_2O content, (2) SiO_2 remains unchanged except in the outermost rind of sample 38d, (3) total iron ($Fe_2O_3^T$) and K_2O values generally increase, (4) MgO and Al_2O_3 behave erratically (Appendix B), (5) TiO_2, Na_2O and P_2O_5

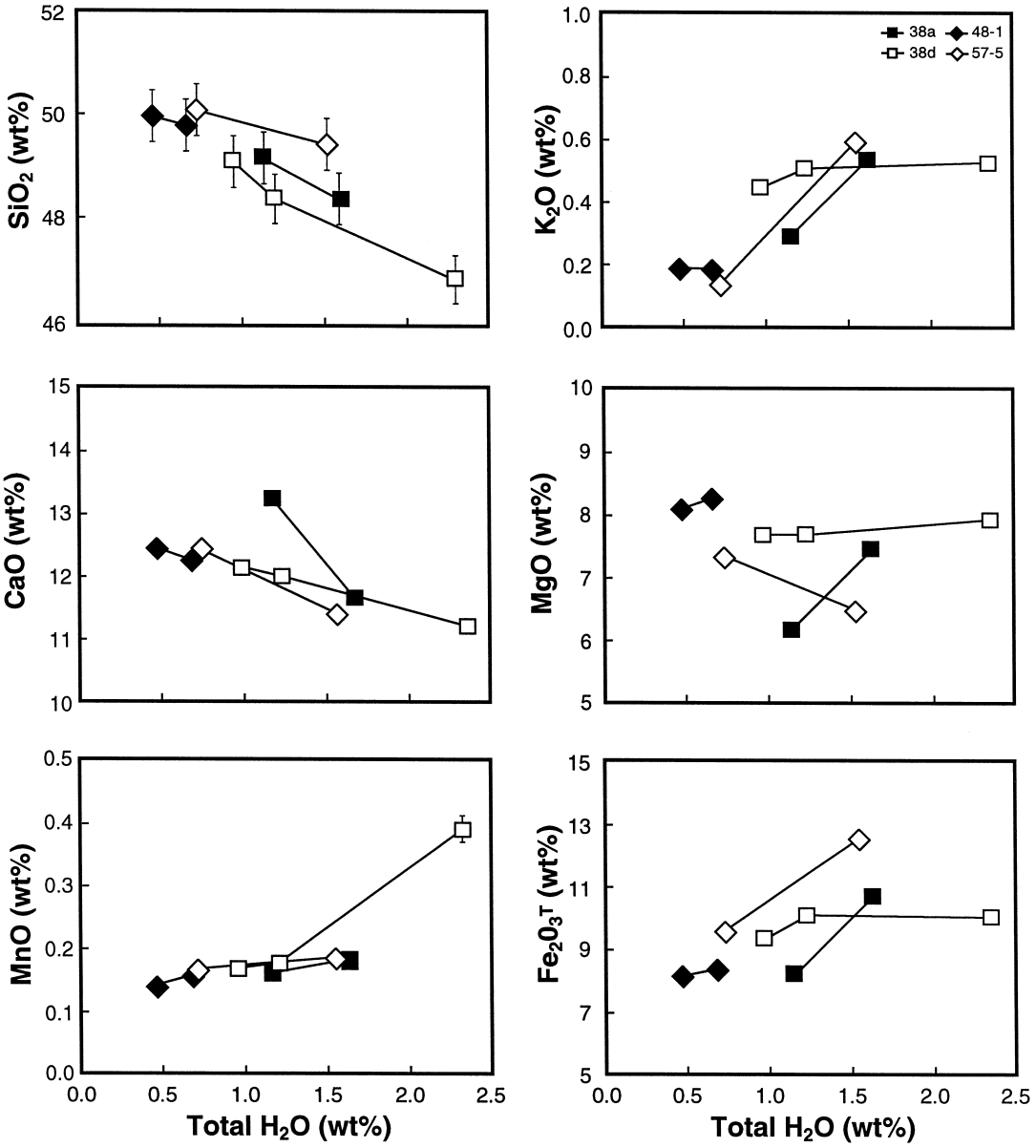

Fig. 5. SiO_2, CaO $Fe_2O_3^T$, MgO, MnO and K_2O plotted vs. H_2O content for the distinct alteration halos of samples 38a, 38d, 48-1 and 57-5. In displayed trends the left data point always represents the rock interior (less altered) and the right the outermost alteration halo (more altered). The maximum analytical error is represented either by error bars or by the size of the data point.

remain unchanged and (6) Fe^{3+}/Fe^{T} ratios consistently increase (Fig. 6). This latter correlation can also be extended to visual alteration estimates in hand specimens, suggesting that alteration is generally associated with an increase in oxidation state of iron.

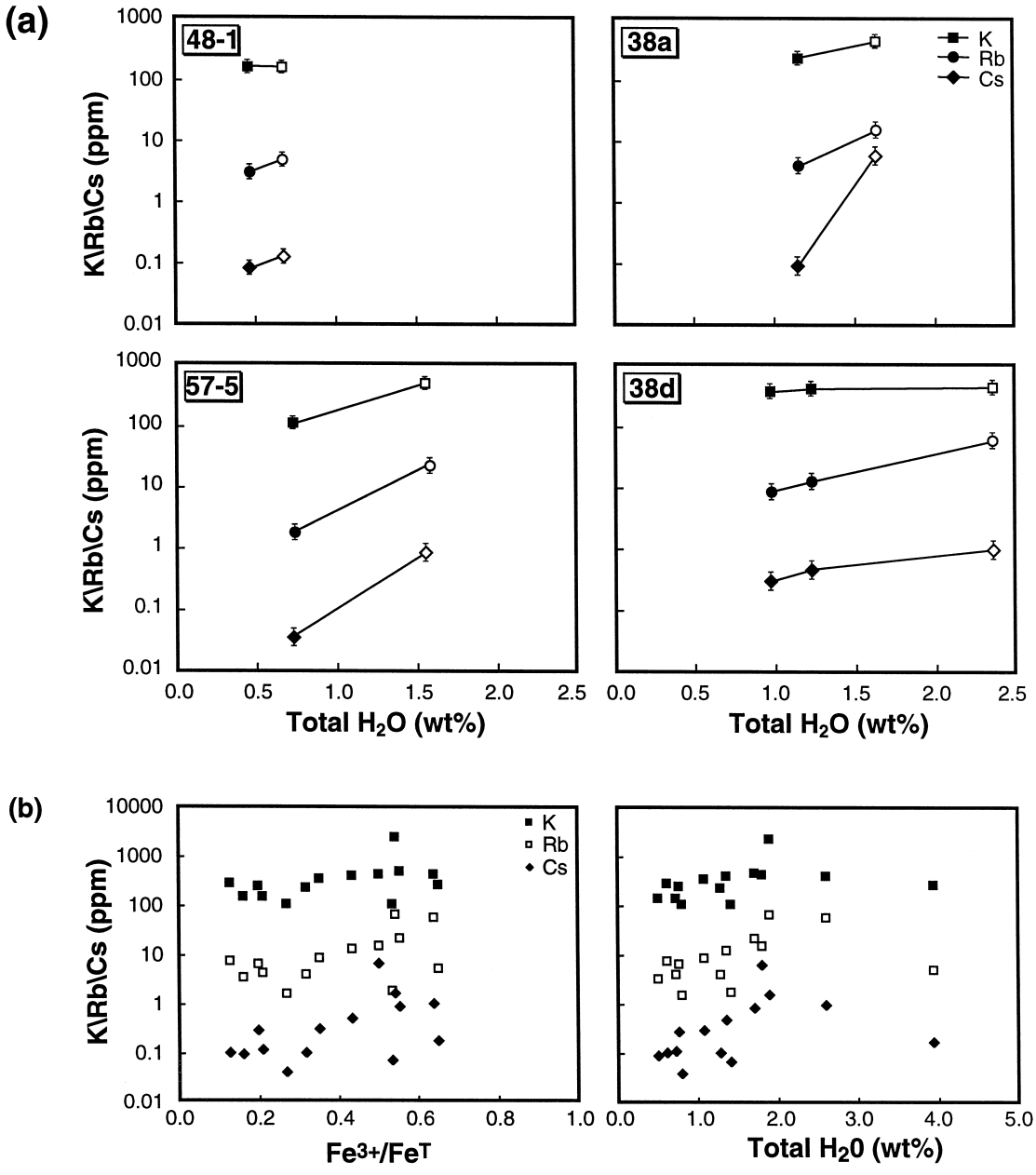

Fig. 6. (a) K, Rb and Cs concentrations for samples 38a, 38d, 48-1 and 57-2 are plotted vs. H_2O content. In displayed trends the filled symbol represents the rock interior and the empty symbol the outermost alteration halo. Error estimates are indicated as in Fig. 5. (b) K, Rb and Cs concentrations for all samples are plotted vs. H_2O content and Fe^{3+}/Fe^{T}.

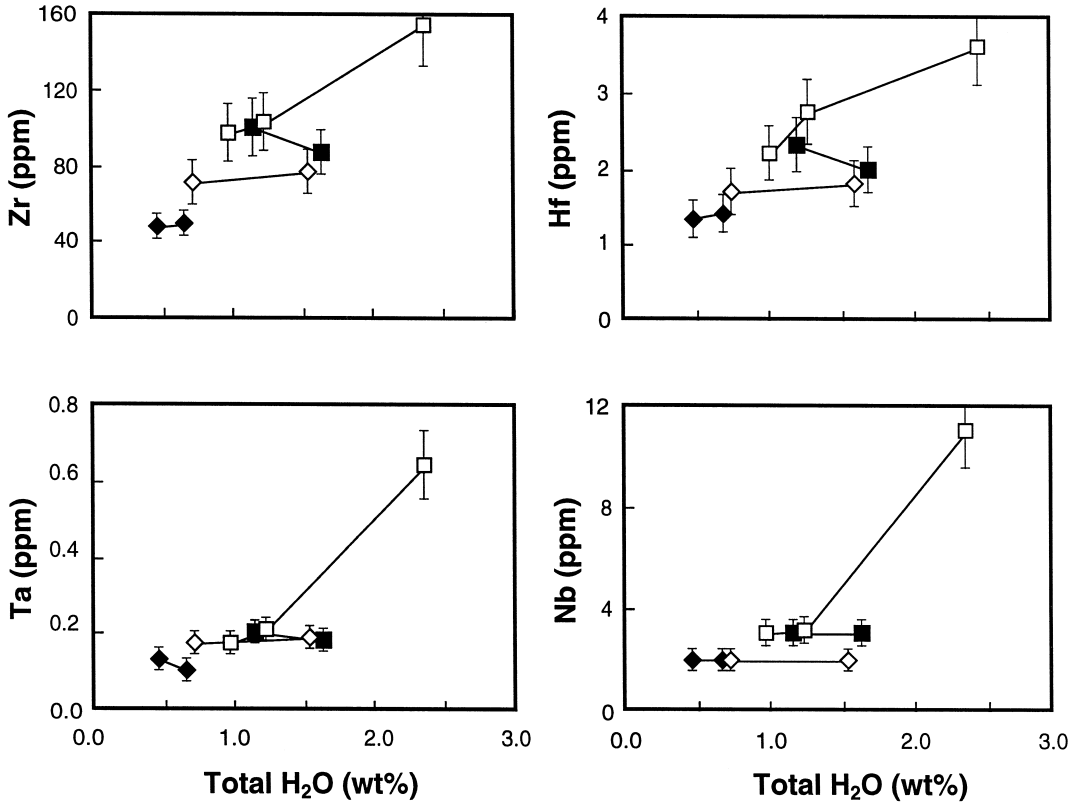

Fig. 7. Nb, Hf, Ta and Zr concentrations for samples 38a, 38d, 48-1 and 57-2 are plotted vs. H_2O content. In displayed trends the filled symbol represents the rock interior and the empty symbol the outermost alteration halo. Error estimates are indicated as in Fig. 5.

K, Rb and Cs concentrations for all samples are given in Appendix B. Samples with distinctive alteration halos are plotted in Fig. 6a. Wherever increases in these elements can be demonstrated, the order of enrichment is always Cs > Rb > K. Other trace elements exhibit erratic behavior with regard to H_2O content (Fig. 7). Ba, Zr, Hf, Ta, Nb and Y show up to threefold enrichment in the outermost zone of sample 38d relative to values in the adjacent alteration zone. These increases are also positively correlated with Mn concentrations and the presence of secondary Mn-oxyhydroxide. These trace elements appear to have been sequestered during the precipitation of a rind of Mn-hydroxides.

North American Shale Composite (NASC) normalized REE compositions for samples with distinct alteration halos are plotted in Fig. 8. Samples 38a, 48-1 and 57-5 did not exhibit any obvious changes beyond a possible analytical error. Sample 38d, on the other hand, did show substantial LREE and minor HREE enrichment in its outermost zone (38d A) with the exception of Eu concentrations which did not change.

5. Discussion

5.1. Formation of secondary minerals

During the initial phase of weathering, particularly under low temperature conditions, amorphous phases can form as a first step between the original rock minerals and new secondary minerals (Eggleton and Keller, 1982). For example, amorphous allophane has been shown to form at an early weathering stage of basic silicate material and persists in the soil provided that conditions remain acidic (Fields and

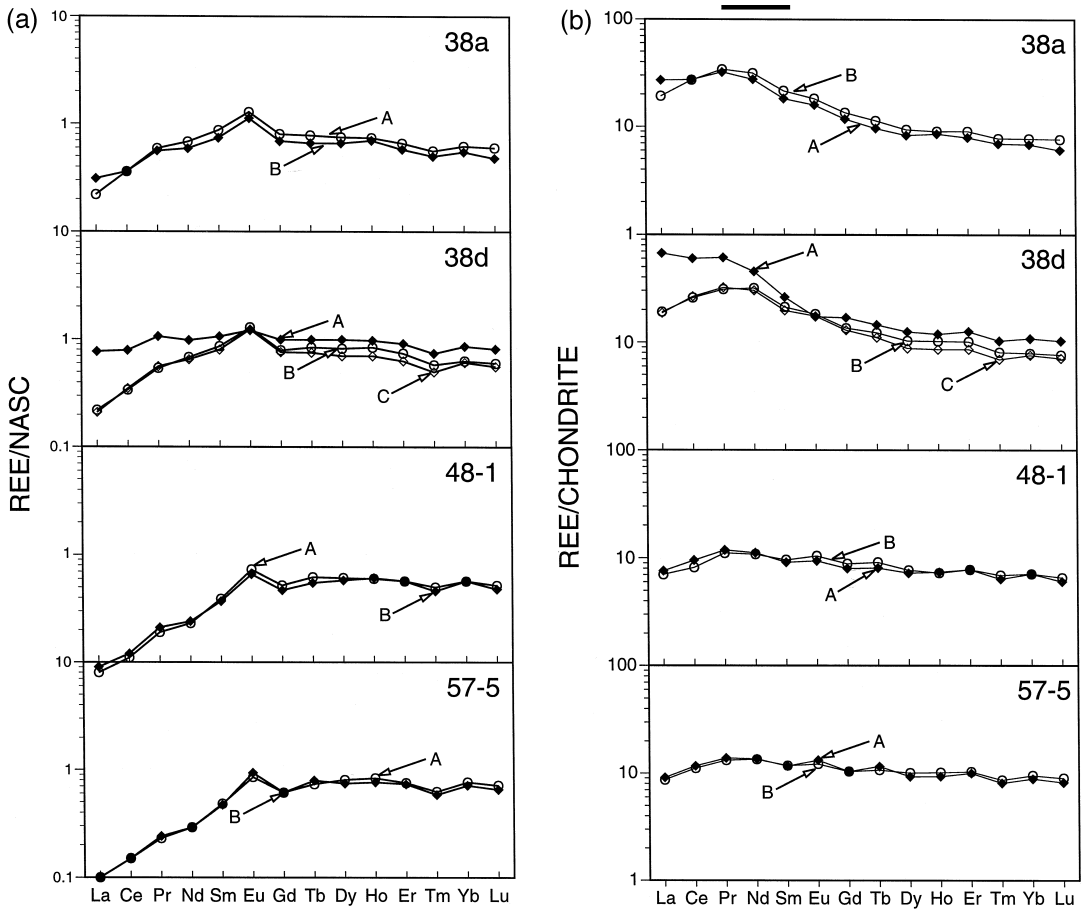

Fig. 8. (a) NASC (North American Shale Composite) normalized REE patterns for samples with distinct alteration zonations. NASC values are from Haskin et al. (1968). (b) Chondrite normalized REE patterns for samples with distinct alteration zonations. Chondrite values are from Taylor and McLennan (1985).

Claridge, 1975). The absence of celadonite peaks in XRD scans of samples in the present study suggests that celadonite/Fe-oxyhydroxide plays a similar role. Development of a crystalline phases may have been prohibited due to either an excess of Fe^{3+} or deficit of Mg^{2+} to sufficiently balance the incorporation of K^{+} to form a true celadonite phase.

Very poorly crystallized yellowish secondary mineral assemblages (palagonite) can replace basaltic glass (Honnorez, 1981). Palagonites have variable composition, and many have smectite as their only crystalline component (Stokes, 1971; Honnorez, 1981; Eggleton and Keller, 1982). Eggleton and Keller (1982) described palagonite as the transitional phase between volcanic glass and smectite during alteration. Smectite, however, may not always be the end product during glass alteration, because, as mentioned previously, celadonites and Fe-oxyhydroxides were the only recognized secondary minerals in a zone of oxidative alteration (Bass, 1976; Andrews, 1980). This suggests that the celadonite/Fe-oxyhydroxide described here could be equivalent to palagonite, i.e., a transitional assemblage between basaltic glass and secondary celadonite.

High FeO and low K_2O contents in celadonites have been interpreted to be the result of mixing between celadonite and nontronite (Stakes and Scheidegger, 1981; Alt and Honnorez, 1984). However, the mixtures observed here show no XRD evidence of nontronite. Structural formulae calcu-

lated from microprobe data have octahedral totals too high to be consistent with a mixture of two di-octahedral minerals. Weaver and Pollard (1975) noted that, in the case of celadonite, some of the cations in excess of 2.00 assigned to the octahedral sheet could equally be assigned to the interlayer (either as ions or in a hydroxide layer). This may, in part, account for the unusual octahedral totals observed in celadonite/Fe-oxyhydroxide. Celadonite/Fe-oxyhydroxide (although X-ray amorphous) is chemically closest to a true celadonite, e.g., lowest octahedral total, low FeO and high K_2O (Table 2 and Appendix A).

5.1.1. Oxidative alteration

Celadonite/Fe-oxyhydroxide and Fe-oxyhydroxide are principally confined to alteration zones immediately adjacent to cracks connected directly to the sample surface, or immediately adjacent to the sample surface. We, therefore, suggest that these minerals formed at high water/rock ratios (Boehlke et al., 1984) in a zone of oxidative diagenesis, where: (1) ferric oxides (e.g., goethite, limonite and hematite) and celadonite can stably exist (Seyfried et al., 1978), (2) celadonite rarely, if ever, exists as a pure phase (Buckley et al., 1978; Andrews, 1980), (3) celadonite forms at temperatures generally less than 26°C (Kastner and Gieskes, 1976; Seyfried and Bischoff, 1979), and (4) there is an absence of chlorite, epidote or albite that might suggest higher temperatures. The absence of a true celadonite in our samples may be the result of (a) not sufficient time of formation and/or (b) too high water/rock ratios. These samples were collected by dredging, meaning that they are relatively young (no sediment cover) and therefore, were exposed directly to seawater up to the point of sampling. This sets them apart from samples that were collected by drilling, i.e., from below a sediment cover. Only very young drilled basalts show similar features (Laverne and Vivier, 1983; Adamson and Richards, 1990).

We have observed the following secondary mineral assemblages in the zone of oxidative alteration: (1) Fe-oxyhydroxides filling vesicles and minor cracks, (2) celadonite/Fe-oxyhydroxide replacing interstitial glass, (3) celadonite/Fe-oxyhydroxide replacing Fe-oxyhydroxides in vesicles and voids (Fig. 5), and (4) replacement of secondary saponite. The alteration of glass is assumed to represent the earliest stage of alteration, glass being more reactive than the surrounding ferromagnesian phases. The formation of celadonite/Fe-oxyhydroxide (observation a) is facilitated by cations already available in the glass and may involve an atom-by-atom reconstitution of glass into secondary minerals. The process must also be accompanied by oxidation of ferrous iron by oxygenated seawater (Seyfried et al., 1978):

$$4Fe^{2+} + O_2 + 6H_2O = 4FeOOH + 8H^+ \quad (1)$$

a reaction that generates protons, thus enhancing the stability of celadonite and Fe-oxyhydroxides and impairing the stability of carbonates and ferric silicates. In vesicles, the availability of cations is more limited due to the absence of glass and oxygenated seawater may be undersaturated with respect to celadonite. Fe-oxyhydroxides may then precipitate without celadonite (observation b) as a consequence of small changes in pH.

The continuous decrease in water±rock ratio and oxygen fugacity towards the sample interior may account for the observed zonation, typically arranged in the sequence Fe-oxyhydroxide → celadonite/Fe-oxyhydroxide → saponite, proceeding inwards from a crack or the rock surface (e.g., Andrews, 1980). Following precipitation of Fe-oxyhydroxide and a decrease in water±rock ratio and oxygen fugacity addition of K^+, Mg^{2+} and SiO_2(aq) initiate the replacement of Fe-oxyhydroxide by celadonite/Fe-oxyhydroxide. The negative charge balance required for K^+ uptake is provided through substitution of seawater-derived Mg^{2+} for Fe^{3+}. The fixation of SiO_2(aq) onto a layered hydroxide sheet explains natural and synthetic neoformation of clay minerals (Henin, 1956). Synchronously, deeper within the sample, celadonite/Fe-oxyhydroxide replaces saponite that originally formed under reducing conditions. For example, sample 57-2, which is pervasively altered, contains celadonite/Fe-oxyhydroxide that replaces saponite (Fig. 3b), indicating a change from reducing to oxidizing conditions. Oxidation of Fe^{2+} to Fe^{3+} allows incorporation of potassium into the saponite structure and initiates transformation into celadonite/Fe-oxyhydroxide.

5.1.2. Non-oxidative alteration

After reaction in the zone of oxidative alteration, seawater will be depleted in oxygen and potassium, enriched in calcium and, possibly, magnesium. Reaction of this modified seawater with primary minerals produces a zone of non-oxidative diagenesis (Bass, 1976; Seyfried et al., 1978; Andrews, 1980). Bass (1976) emphasized that some oxygen is available in this `non-oxidizing' environment, but diffusion rates are slow enough to allow Fe^{3+} incorporation into sheet silicates and little, if any, Fe^{3+} remains for oxide formation. Alteration reactions in this zone cause precipitation of saponite and calcite at low temperatures (Bass, 1976; Seyfried et al., 1978; Andrews, 1980; Honnorez, 1981; Alt and Honnorez, 1984; Thompson, 1991; Alt et al., 1992; Gallahan and Duncan, 1994). Saponites show substantial amounts of Mg^{2+} in their structure and if the pH of a smectite±seawater system rises above 8.5 the following reaction can remove magnesium from the aqueous phase (Henin, 1956; Drever, 1974; Seyfried et al., 1978):

$$Mg^{2+} + 2OH^{-} + \text{smectite} = Mg(OH)_2 \pm \text{smectite} \quad (2)$$

In samples which exhibit distinct alteration zones saponite is confined to the sample interior, i.e., zone of non-oxidative diagenesis, where it replaces intersertal groundmass (microcrystalline and glassy) and to a zone where it replaces celadonite/Fe-oxyhydroxide. This latter zone is best described as a transition zone between oxidative and non-oxidative alteration, where without sufficient recharge of fresh oxygenated seawater, conditions become progressively reducing and celadonite/Fe-oxyhydroxide becomes unstable. Saponites in this zone usually show higher Fe and K values than saponites in the zone of non-oxidative alteration. Furthermore, this zone is characterized by a material (mineral or mineral mixture?) that appears to be transitional between celadonite/Fe-oxyhydroxide and saponite (Fig. 3b, Fig. 4, Table 2). Similar replacement reactions have been observed in earlier studies, however the direction of replacement was unclear. Alt and Honnorez (1984) reported a formation sequence of first celadonite±nontronite followed by saponite, whereas Stakes and Scheidegger (1981) reported replacement of saponite with celadonite±nontronite. New evidence from samples 38a and 57-2 suggests that the direction of reaction is controlled by the redox state, e.g., H_2O content or Fe^{3+}/Fe^{T}. Saponite replaces celadonite/Fe-oxyhydroxide in the less altered sample (38a), whereas in the more altered sample (57-2) celadonite/Fe-oxyhydroxide replaces saponite.

5.2. Chemical changes in samples with distinct alteration zones

5.2.1. Major elements

In order to further examine alteration trends, samples that display a distinct alteration zonation are valuable. In general, the compositional changes detected in this study are similar to those observed in previous studies of seafloor alteration (Fig. 5). The increase in $Fe_2O_3^T$ cannot be explained by uptake of Fe from seawater, but the breakdown of volcanic glass could be one source of additional Fe. Alt (1993), who observed a similar increase in $Fe_2O_3^T$, suggested that Fe may also be derived from a deeper source in the volcanic pile, possibly at higher temperatures. The increases observed in samples from this study, however, are more likely caused by Fe mobility under reducing conditions in the sample interior, followed by precipitation under oxidizing conditions in the outer zone. Al_2O_3 tends to decrease with increasing alteration. The same trend can be recognized in secondary minerals. For example, saponite, which has higher Al contents than celadonite/Fe-oxyhydroxide, occurs mainly in the higher Al_2O_3 zone within the rock interiors.

Slight decreases in of Al_2O_3, CaO and Na_2O in the outer zones are probably due to alteration of plagioclase and glassy groundmass material (Staudigel and Hart, 1983; Alt, 1993). The behavior of MgO has been reported to depend in part on the degree of alteration (Thompson, 1973, 1991); decreases have been attributed to an early breakdown of olivine and subsequent SiO_2 and MgO loss to seawater. In sample 38a-A celadonite/Fe-oxyhydroxide is partly replaced by saponite which may account for the increase in MgO.

In general the observed major element behavior is in good agreement with mineralogical changes (Fig. 5). SiO_2 and $Fe_2O_3^T$ are higher in the sample interiors where saponite and celadonite/Fe-oxyhydroxide

are the dominant alteration minerals, whereas K_2O increases towards the sample surface in samples that contain more celadonite/Fe-oxyhydroxide than Fe-oxyhydroxide.

5.2.2. Trace elements

The behavior of trace elements during low-temperature alteration is still poorly understood. Honnorez (1981), who reviewed a variety of low-temperature alteration studies noted that the only consensus was enrichments in Rb and Cs in altered rocks. There is considerably less agreement regarding the immobility of Zr, Nb, Hf and Ta during low-temperature alteration (Bienvenu et al., 1990). They are generally thought to be immobile and, therefore, an enrichment is generally interpreted as passive accumulation due to a loss of mass during alteration. The enrichment of Zr, Nb, Hf and Ta in the outermost zone of sample 38d (38d-A) cannot be explained by simple mass loss, because this sample is not altered enough. In our suite of samples these trace elements are positively correlated with Mn (Appendix B) which warrants the assumption that the formation of Mn-oxyhydroxides may play a role in their enrichment. The outermost zone of sample 38d (38d-A) contains minor amounts of Mn-oxyhydroxides, thus Zr, Nb, Hf and Ta (Fig. 7) could have been derived from seawater during extreme alteration conditions, i.e., very high water/rock and oxygen fugacity. This uptake would be similar to the trace element enrichment found in manganese nodules and crusts (e.g., Hein et al., 1996).

Scavenging of elements into and onto metal hydroxides results from: (1) coprecipitation, (2) adsorption, (3) surface complex formation, (4) ion exchange, and (5) penetration of the crystal lattice (Chao and Theobald, 1976). Adsorption, however, has been observed to be the basis of most surface-chemical reactions (Stumm and Morgan, 1996) making it the most likely cause for the high trace element concentrations in sample 38d. Fe/Mn-oxyhydroxides, precipitated on or near the sample surface, can scavenge large concentrations of elements from seawater; the high water±rock ratio compensates for low trace element concentrations in seawater.

Little information exists regarding the intensity of scavenging of elements other than the heavy or ore metals. However, many metals that form strong OH-complexes in water also bind strongly to hydroxides (Dzombak and Morel, 1990) and most of the trace elements enriched in sample 38d-A form strong OH-complexes. Small changes in pH can result in large changes in adsorption efficiency onto Fe- and Mn-hydroxides (e.g., Stumm and Morgan, 1996). A change in pH may be due to sample oxidation (see reaction [1]) and/or mixing of altered and fresh seawater near the sample surface.

Trace and rare earth elements are enriched in 38d-A but not in other samples. This may reflect the relatively high Mn concentration in sample 38d-A which is probably present as Mn-oxyhydroxide. Mn-oxyhydroxide has a much greater reactivity than Fe-oxyhydroxide which can result from several factors: (1) Mn can exist in several oxidation states, (2) it forms non-stoichiometric oxides with variable valence states, (3) Mn-oxides exist in several crystalline or pseudo crystalline forms, and (4) Mn-oxides form co-precipitates and solid solutions with Fe-oxides (Ponnamperuma et al., 1969). In addition, Mn-oxyhydroxides may have surface areas much bigger than those of Fe-oxyhydroxides (Morgan and Stumm, 1964), thus enhancing their scavenging efficiency.

5.2.3. Rb and Cs

Rb and Cs together with K are discussed separately from the other trace elements because of their similar chemical behavior and their susceptibility to low-temperature alteration. K, Rb and Cs are among the most incompatible elements (Sun and McDonough, 1989) and, therefore, show a very low abundance in most mid-ocean ridge basalt. During alteration, their concentration can easily increase because they are readily supplied by seawater and incorporated in, or adsorbed on, secondary clay minerals (Hart et al., 1974). Hart (1969) observed that substantial K, Rb and Cs enrichment can occur before the water content reaches a level which would normally be considered diagnostic for alteration. In our study K, Rb and Cs are such sensitive indicators of alteration that similar enrichment trends can be observed in both individual samples (Fig. 6a) and all samples relative to each other (Fig. 6b) independent of their initial K, Rb and Cs concentration.

The trends plotted in Fig. 6a are consistent with observations made in earlier studies of altered oceanic

basalt (Hart, 1969; Thompson, 1973; Hart et al., 1974; Honnorez, 1981). The sensitivity to alteration increases, in general, in the order K > Rb > Cs. A slightly reversed trend can be observed for very altered samples; values decrease with increasing alteration (Fig. 6a,b). One explanation might be that in pervasively altered samples, where no distinct alteration zonation exists, values for K, Rb and Cs represent an average value for the whole rock. Higher values in other samples are usually confined to the outermost alteration zone, i.e., zone of high water to rock ratio. Since K, Rb and Cs are exclusively supplied by seawater, the water to rock ratio should be the main factor controlling the enrichment of these elements. Hart (1969) suggested that the depletion of formerly added alkalis in altered basalt might be controlled by the degree of alteration and that, under very severe conditions, the alkalis might be leached from the basalt.

5.2.4. Rare earth elements

The positive Ce anomaly in 38d-CR (Fig. 9) and the general increase in Ce concentrations in all altered samples is consistent with the fractionation of Ce^{4+} from the trivalent REE during uptake of the REE from seawater by secondary phases (Ludden and Thompson, 1978). The positive correlation between Mn and Ce (Appendix B) suggests that this fractionation is largely due to selective adsorption of Ce^{4+} by Fe±Mn oxyhydroxides. Cerium (Ce^{4+}) forms colloidal ceric hydroxide which is relatively easier scavenged by Fe/Mn-oxyhydroxides than Ce^{3+} (Carpenter and Grant, 1967). There is also a fractionation of the light REE (LREE) from the heavy REE (HREE) during alteration which presumably is due to selective exchange of REE with seawater. The concentrations of REE in seawater are 4 to 6 orders of magnitude lower than in basaltic rocks (e.g., Fleet, 1984). Consequently, equilibrium exchange reactions involving seawater and secondary minerals will lower the REE concentrations in altered basalts unless the water/rock ratios are unrealistically high. This does not seem to be the case for the altered samples studied here, suggesting that the REE may be quantitatively removed from seawater by adsorption exchange reactions on secondary mineral surfaces, particularly oxyhydroxides. The fractionation of LREE and the lack of an overall

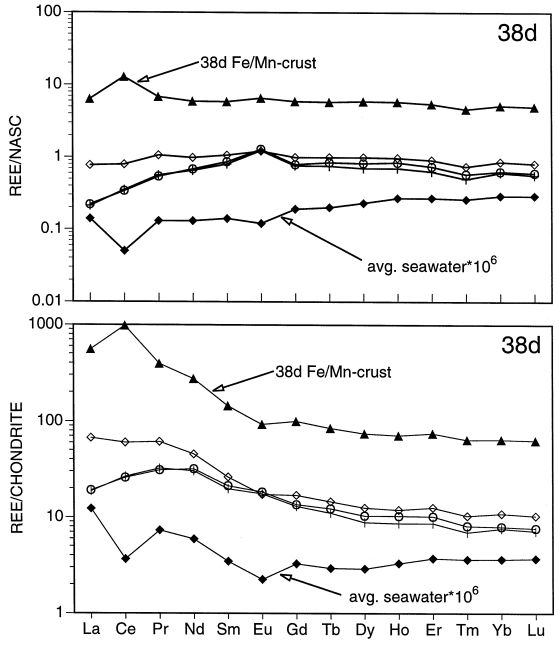

Fig. 9. NASC (North American Shale Composite) and chondrite normalized REE patterns for sample 38d including zones A, B, and C. 38d-CR is a Mn-rich Fe-crust coating the sample. Seawater concentrations are from Fleet (1984).

REE depletion during alteration suggests that the stability of the REE in seawater may vary as a function of mass, perhaps as a result of the presence of more stable HREE carbonate complexes in seawater (Lee and Byrne, 1993). This variability in REE complex stability in seawater will be reflected in the adsorption partition coefficient for each REE. It is also interesting to suggest that at ambient seawater temperatures the REE content of basalts may increase as a result of adsorption from seawater but may then decrease at higher temperatures where hydroxides and oxyhydroxides are thermally unstable and where residence sites for REE are not present.

5.3. Alteration through time

Mineralogic changes during the weathering of oceanic basalt should, in part, reflect the local redox conditions. Honnorez (1981) and Thompson (1991), in reviews of low-temperature weathering of oceanic basalt, have established differences in secondary

mineralogy between dredged and drilled basalt. They concluded that dredged basalt weathered under oxidative conditions resulting from high water±rock ratios, whereas drilled basalt weathered under more reduced conditions as a consequence of lower water±rock ratios. However, in the earliest stages of weathering, dredged basalt show mineralogic zoning trends that result from both oxidative and non-oxidative conditions. It is only with more advanced weathering that there is a gradual overprinting of the non-oxidative assemblages by oxidative assemblages. Thus, the samples described here form a microcosm of processes that encompass both dredged and drilled basalt, and allow a detailed description of the gradual changes occurring during weathering.

The basalt±seawater system physically involves a decrease in water±rock ratio as a function of distance from the basalt±seawater interface, assuming that rock permeability also decreases in this direction. This situation applies at different scales, ranging from a hand specimen to the oceanic crust as a whole. The extent of chemical reactivity in this system is a function of: (a) water±rock ratio, (b) solution chemistry, and (c) rock texture (e.g., Seyfried and Bischoff, 1979). Regarding the latter, decrease in reactive glass matrix and the coarsening of texture

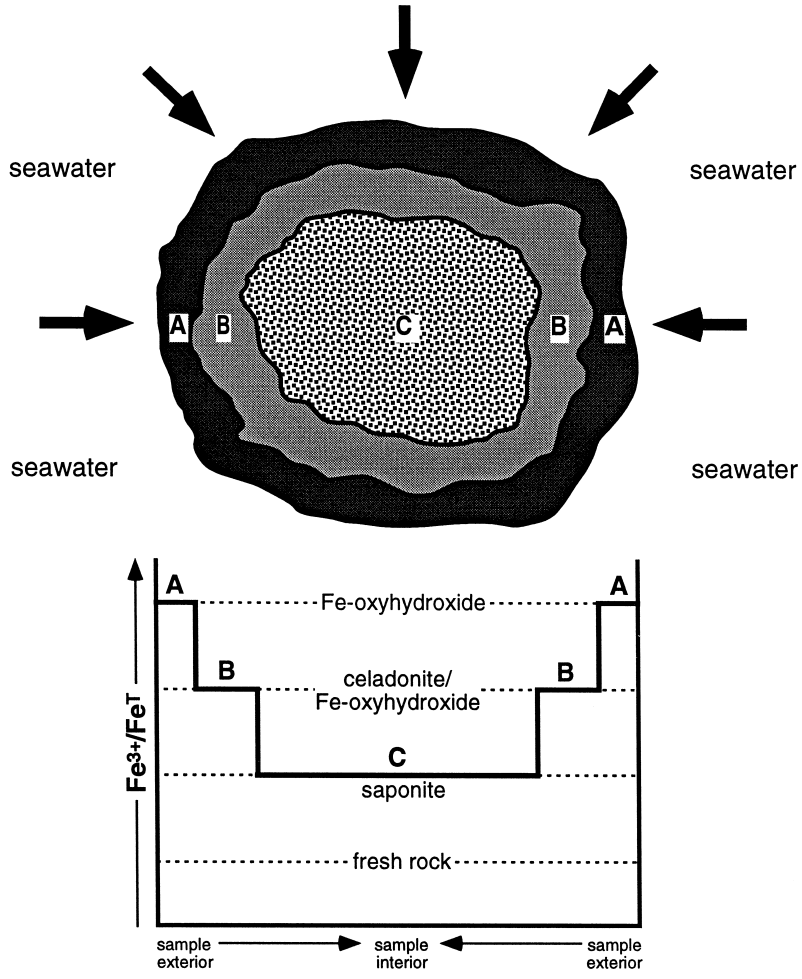

Fig. 10. Graphical display of a theoretical seawater rock system. Alteration zones A, B and C are plotted vs. increasing oxidation state. Dashed lines indicate relative stability areas for secondary minerals. For further explanation, see text.

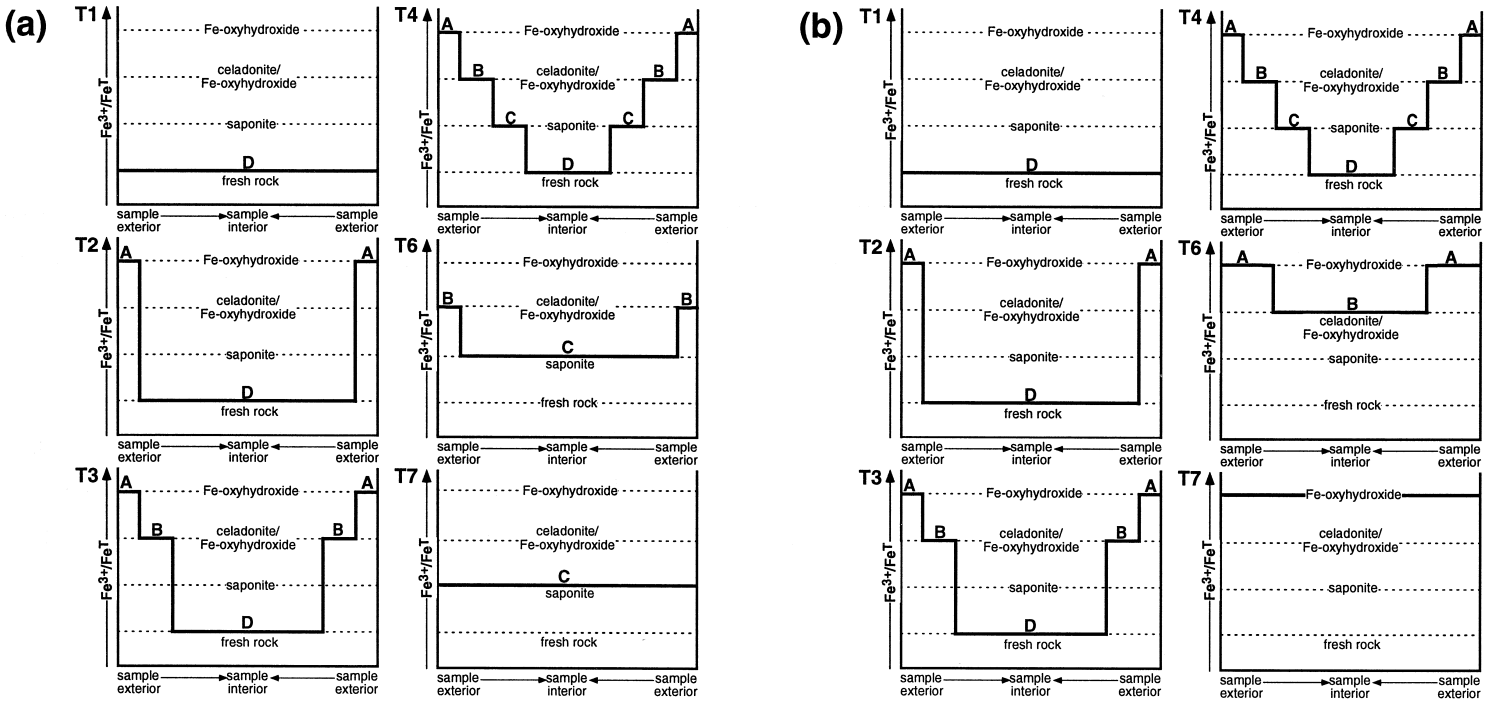

Fig. 11. (a) Evolution of a theoretical seawater±rock system through time (T1±T7), where the rock becomes separated from direct contact with seawater. T5 is represented in Fig. 9. (b) Evolution of a theoretical seawater±rock system through time (T1±T7), where the rock remains in direct contact with seawater. T5 is represented in (a).

have a profound effect on chemical reactivity. Glassy matrix is enhanced at the chilled margins of submarine flows, so chemical reactivity will be enhanced at the rock±seawater interface. However, changing solution composition as the seawater migrates into the rock may enhance reactions within the rock interior. The combination of these properties result in the development of a distinct mineralogic zoning during the early stages of weathering (Fig. 10). This zonation is formed by the progressive inward movement of small volumes of seawater along mineral fractures and grain boundaries. The initial reaction of the glass-rich, fresh outer rind of basalt with oxygenated seawater results in conversion of Fe^{2+} to Fe^{3+}, local decrease in solution pH, and hydration of glass. At this stage, secondary minerals are not precipitated in primary pore space, but glass may begin to devitrify and alter during hydration without substantial cation mobility. This initial solution packet, now with a slightly lower pH and lower oxygen content than seawater, progresses further inward along microfractures. Gradual reaction with glass matrix, ferromagnesian minerals (olivine, pyroxene) and Fe±Ti oxides enriches the solution in Ca, Fe, and Mg and also leads to alteration of primary minerals and some precipitation of secondary minerals in primary pore spaces. These secondary assemblages are dominantly saponitic, reflecting the non-oxidative condition of the fluid and low water±rock ratios.

At this stage a large chemical gradient exists between seawater and the solution front penetrating the rock. Thus, the slow physical movement of fluid into the rock is accompanied by chemical diffusion of cations into and out of the rock. For instance, Fe is expected to diffuse toward the seawater interface, whereas Mg and Ca may diffuse in the opposite direction. The result of diffusion of cations toward the seawater interface is to enrich the oxidative zone of alteration in these cations and enhance the precipitation of Fe^{3+}-bearing minerals, e.g., Fe-oxyhydroxides and celadonite in primary pore spaces and fractures.

Conversion of Fe^{2+} to Fe^{3+} and precipitation of Fe^{3+}-rich secondary minerals in the outermost glassy rind provides an outermost oxidative zone in which further oxidation of Fe^{2+} is not possible. If this process results in a permanent loss or a substantial reduction in rock permeability, i.e., the supply of fresh seawater to the water±rock system is cut-off or substantially diminished, then the mineralogic zoning may be preserved or alteration may proceed under reducing conditions (Fig. 11a). If permeability is maintained, or new permeability created, then fresh, oxygen-bearing seawater penetrates further into the rock before encountering reduced Fe. The process of iron oxidation is then repeated and the oxidative front moves inward, overprinting previous zones of non-oxidative minerals. With sufficient time, the final secondary mineral assemblage would be dominated by Fe-oxyhydroxides, with little or no evidence for the non-oxidative paragenesis (Fig. 11b).

In summary, we consider the secondary mineral assemblages observed in these samples evidence for a zoned alteration system that reflects solution pH, solution cation concentrations, variable water±rock ratios, and the diffusion of cations into and out of the water±rock system. Physical circulation of solution into and out of the fluid±rock system is unlikely, assuming that fluid movement is dominated by grain boundary diffusion and chemical diffusion through the solid phases. Under these conditions, we propose that seawater entering the rock structure is redistributed in hydrous secondary minerals.

Adamson and Richards (1990), who studied very young basalts that were collected by drilling, proposed an additional interpretation for the saponitic assemblages. They consider an early stage of low temperature hydrothermal alteration (saponite) that is overprinted by a stage of seawater alteration (celadonite). This alteration sequence, however, is not likely for our samples, because no minerals indicative of higher temperature alteration were found.

6. Summary and conclusions

(1) Mineralogical and chemical changes are comparable with results from other studies of seafloor alteration at low-temperatures. H_2O, K, Rb, Cs and $Fe_2O_3^T$ are added and cao and SiO_2 are removed from the rock.

(2) The exterior formation of Mn-rich Fe-crusts and the interior precipitation of Mn-rich Fe-oxyhydroxides are important chemical processes controlling the behavior of some trace elements such as REE, Ba, Zr, Hf, Ta, Nb, and Mo.

Appendix A
Morphology and macroscopic alteration features of rock samples collected during the Southern CROSS cruise

Sample	Morphology	Texture	Vesicles	Alteration
11-4	pillow	phyric	unfilled	oxidized surface and cracks, fresh interior, fresh phenocrysts
14-3	pillow	sparsely phyric	unfilled	oxidized surface and cracks, fresh interior, fresh phenocrysts
14-8	pillow	sparsely phyric	unfilled	oxidized surface and cracks, fresh interior, fresh phenocrysts
28	pillow	sparsely phyric	unfilled	oxidized surface and cracks, fresh interior, fresh phenocrysts
38a	massive	glomeroph. plag 1±3 mm, gm: inters. w/ plag needles	none	Mn-crust, oxidized surface, centripetal oriented alteration zones: A, 0.5±1 cm, brownish gray; B, gray
38b	massive	glomeroph. plag 1±3 mm, gm: inters. w/ plag needles	coated	Mn-crust, oxidized surface, centripetal oriented alteration zones: A, 0±1 cm, gray; B, 1±1.7 cm, yellowish brown; C, 1.7±2 cm dark gray; D, gray
38d	massive	glomeroph. plag 1±3 mm, gm: inters. w/ plag needles	partly filled	Mn-crust, oxidized surface, centripetal oriented alteration zones: A, 0.5±1.5 cm, yellowish brown; B, 1.5±2.5 cm, gray; C, 2.5±2.9 cm, dark gray; D, gray
43	pillow	sparsely phyric	unfilled	oxidized surface, no visible phenocryst alteration
48-1	massive	glomeroph. plag 1±3 mm, gm: inters. w/ plag needles	partly filled	Mn-crust, oxidized surface, centripetal oriented alteration zones: A, 0.2±1.5 cm, brownish gray; B, gray
50-5	pillow	glomeroph. plag 1 mm, gm: inters. w/ plag needles	partly filled	oxidized surface, phenocrysts partly altered, centripetal oriented alteration zones: A, 0.3±1 cm, dark gray; B, gray
57-2	massive	glomeroph. plag 1±3 mm, gm: inters. w/ plag needles	none	Mn-crust, pervasively altered
57-5	massive	glomeroph. plag 1.5 mm, gm: inters. to holo-crystalline	partly filled	Mn-crust, centripetal oriented alteration zones: A, 0.2±0.3 cm, brownish gray; B, 0.3±1.8 cm, dark gray; C, gray w/ plag needles
57-7	massive	glomeroph. plag 1±5 mm, gm: inters w/ plag needles	partly filled	Mn-crust, pervasively altered, phenocrysts seem to be completely replaced
66-9	pillow	variolitic. plag 1 mm, gm: inters. w/ spherulitic plag	partly filled	oxidized surface and cracks

Appendix B

Chemical compositions for whole-rock powders. In samples where distinct alteration zones were recognized, these zones were designated successively inward in alphabetical order, i.e., A → B → C

Sample:	38a A	38a B	38d A	38d B	38d C	48-1 A	48-1 B	50-5	57-2	57-5 A	57-5 B	57-7	66-9	38d-CR
Type:	basalt	basalt	basalt	basalt	basalt	basalt	basalt	basalt	basalt	basalt	basalt	basalt	basalt	Mn-crust
Colour:	brownish gray	gray	brownish gray	dark gray	gray	brownish gray	gray	gray	yellowish brown	brownish gray	dark gray	light brown	light gray	dark brown
SiO_2	48.40	49.15	46.78	48.37	49.10	49.77	49.98	50.48	47.77	49.46	50.10	46.87	49.20	10.54
TiO_2	1.10	1.17	0.94	1.09	1.14	0.93	0.93	1.37	1.32	1.25	1.35	0.67	1.20	1.477
Al_2O_3	15.59	16.92	17.47	16.23	16.29	17.31	17.60	15.20	15.47	14.38	15.55	22.59	16.47	2.56
$Fe_2O_3^T$	10.68	8.25	9.99	10.11	9.35	8.38	8.12	10.25	10.23	12.54	9.59	7.86	9.95	26.55
MnO	0.18	0.16	0.39	0.18	0.16	0.16	0.14	0.17	0.22	0.18	0.17	0.13	0.17	1.77
MgO	7.48	6.16	7.93	7.69	7.68	8.24	8.13	7.45	7.02	6.47	7.34	3.55	8.30	17.03
CaO	11.71	13.26	11.18	11.98	12.19	12.27	12.43	11.34	10.57	11.41	12.44	14.95	11.18	3.06
Na_2O	2.61	2.89	2.60	2.62	2.70	2.38	2.48	2.57	2.76	2.68	2.77	2.04	2.79	1.83
K_2O	0.53	0.28	0.52	0.50	0.44	0.18	0.18	0.31	0.33	0.59	0.13	0.13	0.35	0.29
P_2O_5	0.15	0.16	0.19	0.17	0.16	0.11	0.11	0.16	0.19	0.14	0.15	0.14	0.16	1.248
LOI	1.22	1.14	1.81	0.62	0.50	0.06	0.06	0.14	3.79	0.85	0.05	0.86	0.00	29.66
Total	99.65	99.54	99.80	99.55	99.71	99.79	100.16	99.44	99.67	99.95	99.64	99.78	99.77	96.02
H_2O^T	1.64	1.16	2.36	1.24	0.98	0.67	0.47	0.69	4.07	1.55	0.73	1.28	0.56	25.2
FeO	5.25	5.28	3.78	5.51	5.73	6.11	6.24	7.55	3.78	5.64	6.51	3.64	7.92	ND
Fe_2O_3	4.85	2.38	5.79	3.99	2.98	1.59	1.19	1.86	6.03	6.27	2.35	3.81	1.15	26.55
Sr	310	350	330	330	330	136	128	138	215	150	152	148	152	ND
Y	17.4	19.4	28	21.1	19.2	15.5	15.9	22.9	18.9	19.6	22.6	12.3	19.5	157.1
Zr	87	99	160	103	96	49	47	74	71	77	70	33	74	436
Nb	3	3	11	3.1	3	2	2	3	7	2	2	1.4	7	41
Mo	2.1	1.1	1.4	6.3	8.4	11.8	4.8	1.1	6.1	7.9	6	8.6	1.4	120.3
Ba	182	133	802	76.9	97	47	44.5	56	129	26	21	15.2	79	1275
Hf	2	2.3	3.6	2.73	2.2	1.4	1.34	1.9	1.7	1.8	1.7	0.86	1.8	5.1
Ta	0.18	0.2	0.64	0.21	0.17	0.1	0.13	0.2	0.37	0.19	0.17	0.23	0.37	0.59
K	440	232	432	415	365	149	149	257	274	490	108	108	291	241
Rb	15.3	4.1	57.8	13.1	8.8	4.3	3.4	6.6	5.2	21.7	1.6	1.8	7.7	0.6
Cs	6.43	0.1	0.99	0.49	0.3	0.11	0.09	0.27	0.17	0.84	0.04	0.07	0.1	0.08

Results for SiO_2, Al_2O_3, MgO, FeO^T, MnO, CaO, Na_2O, K_2O and TiO_2 are in oxide wt.% and for Sr, Y, Zr, Nb, Mo, Ba, Hf, Ta, K, Rb and Cs in ppm.

Appendix C
REE analyses for samples with distinct alteration halos

REE	38a A	38a B	38d A	38d B	38d C	48-1 A	48-1 B	57-5 A	57-5 B	38d-Mn
La	9.91	7.05	24.6	6.99	6.83	2.79	2.58	3.34	3.18	203
Ce	26.19	25.98	57.32	24.69	25.35	9.11	7.82	11.19	10.65	936
Pr	4.41	4.67	8.38	4.23	4.4	1.62	1.52	1.9	1.81	53.86
Nd	19.57	22.38	32.27	22.54	21.48	7.92	7.7	9.66	9.58	195
Sm	4.22	4.98	6.04	4.9	4.55	2.11	2.22	2.69	2.72	33.35
Eu	1.39	1.59	1.5	1.59	1.52	0.82	0.91	1.15	1.06	8.12
Gd	3.61	4.15	5.17	4.13	3.96	2.45	2.71	3.17	3.17	30.68
Tb	0.56	0.66	0.84	0.71	0.64	0.47	0.53	0.67	0.62	4.93
Dy	3.17	3.59	4.76	3.93	3.35	2.77	2.95	3.53	3.83	28.37
Ho	0.73	0.77	1.01	0.87	0.73	0.63	0.62	0.79	0.86	6.06
Er	1.97	2.25	3.11	2.51	2.13	1.94	1.94	2.47	2.55	18.53
Tm	0.25	0.28	0.37	0.29	0.25	0.23	0.25	0.29	0.31	2.31
Yb	1.7	1.92	2.68	1.96	1.88	1.77	1.77	2.19	2.35	16.01
Lu	0.23	0.29	0.39	0.29	0.27	0.23	0.25	0.31	0.34	2.39

(3) Formation of specific secondary minerals is partly controlled by the redox state, which is regulated by the seawater to rock ratio. Celadonite/Fe-oxyhydroxide and Fe-oxyhydroxide form during `oxidative alteration', whereas saponite forms during `non-oxidative alteration'. The final alteration products are also controlled by external factors such as sedimentation rate, formation of a manganese crust, or secondary mineral cementation which may determine redox state changes as alteration progresses.

(4) The primary rock texture is an important factor in determining the extent of alteration and mineral paragenesis during alteration. Microcrystalline and glassy groundmass are more susceptible to low-temperature alteration because of the lack of well-developed crystal structure. Plagioclase and pyroxene phenocrysts remained fresh in all studied samples.

(5) The amorphous secondary mixture celadonite/Fe-oxyhydroxide is considered a variety of palagonite with the stable secondary mineral end-member celadonite, not smectite.

Acknowledgements

This paper was part of T. Pichler's MS Thesis at The Colorado School of Mines. Thanks to Emily Klein and Jill Karsten for giving T. Pichler an opportunity to participate in the Southern CROSS Cruise and allowing him to work and sample freely during the cruise. Ken Esposito, Gene Whitney and Steve Sutley, USGS in Lakewood, provided clay separation, XRD equipment and advise. Ian Jonasson, Ajaz Karim, Kevin Telmer, Kathryn Gillis and an anonymous reviewer are thanked for their constructive comments. T. Pichler was supported by a foreign exchange stipend from the German Ministry of Education.

References

Adamson, A.C., Richards, H.G., 1990. Low-temperature alteration of very young basalts from ODP hole 648B: Seroki Volcano, Mid-Atlantic ridge. Proceedings of the Ocean Drilling Program, Scientific Results 106±109, 181±194.

Alt, J.C., 1993. Low-temperature Alteration of basalts from the Hawaiian Arch, Leg 136. Proceedings of the Ocean Drilling Program, Scientific Results 136, 15±16.

Alt, J.C., Honnorez, J., 1984. Alteration of the upper oceanic crust, DSDP site 417: mineralogy and chemistry. Contributions to Mineralogy and Petrology 87, 149±169.

Alt, J.C., France-Lanord, C., Floyd, P.A., Castillo, P., Galy, A., 1992. Low-temperature hydrothermal alteration of jurassic ocean crust, Site 801. Proceedings of the Ocean Drilling Program Scientific Results 129, 415±427.

Andrews, A.J., 1980. Saponite and cealdonite in layer 2 basalts, DSDP Leg 37. Contributions to Mineralogy and Petrology 73, 323±340.

Bass, M.N., 1976. Secondary minerals in oceanic basalts with special reference to DSDP Leg 34. In: Yeats, R.S., Hart, S.R. (Eds.), Initial Reports of the Deep Sea Drilling Project. U.S. Government Printing Office, Washington, DC, pp. 497±506.

Bienvenu, P., Bougault, H., Joron, J.L., Treuil, M., Dimitriev, L.,

1990. MORB alteration: rare-earth element/non-rare-earth hygromagmaphile element fractionation. Chemical Geology 82, 1±14.
Boehlke, J.K., Alt, J.C., Muehlenbachs, K., 1984. Oxygen isotope±water relations in altered deep-sea basalts: low temperature mineralogical controls. Canadian Journal of Earth Sciences 21, 67±77.
Buckley, H.A., Bevan, J.C., Brown, K.M., Johnson, L.R., Farmer, V.C., 1978. Glauconite and celadonite: two separate mineral species. Mineralogical Magazine 42, 373±382.
Cande, S.C., Leslie, R.B., 1986. Late Cenozoic tectonics of the southern Chile trench. J. Geophys. Res. 91, 471±496.
Carpenter, J.H., Grant, V.E., 1967. Concentration and state of cerium in coastal waters. Journal of Marine Research 25, 228±238.
Chao, T.T., Theobald, J.P.K., 1976. The significance of secondary iron and manganese oxides in geochemical exploration. Economic Geology 71, 1560±1569.
Drever, J.I. (Ed.), 1974. The magnesium problem. The Sea, Vol. 5. Wiley, New York, pp. 337±357.
Dzombak, D.A., Morel, F.M.M., 1990. Surface Complexation Modeling: Hydrous Ferric Oxide. Wiley-Interscience, New York.
Eggleton, R.A., Keller, J., 1982. The palagonitization of limburgite glassÐa TEM study. Neues Jahrbuch der Mineralogie, H 7, 321±336.
Fields, M., Claridge, G.G.C. (Eds.), 1975. Inorganic components. Soil Components, Vol. VII. Springer Verlag.
Fleet, A.J., 1984. Aqueous and sedimentary geochemistry of the rare earth elements. In: Henderson, P. (Ed.), Rare Earth Element Geochemistry. Developments in Geochemistry, Elsevier, Amsterdam, pp. 343±373.
Gallahan, W.E., Duncan, R.A., 1994. Spatial and temporal variability in crystallisation of celadonites within the Troodos Ophiolite, Cyprus: implications for low-temperature alteration of the oceanic crust. Journal of Geophysical Research 99, 3147±3161.
Grant, J.A., 1986. The isocon diagramÐa simple solution to Gresens' equation for metasomatic alteration. Economic Geology 81, 1976±1982.
Gresens, R.L., 1967. Composition±volume relationships of metasomatism. Chemical Geology 2, 47±55.
Hart, R.A., 1969. K, Rb, Cs, contents and K/Rb, K/Cs ratios of fresh and altered submarine basalts. Earth and Planetary Science Letters 6, 295±303.
Hart, R.A., 1970. Chemical exchange between sea water and deep ocean basalts. Earth and Planetary Science Letters 9, 269±279.
Hart, R.A., Erlank, A.J., Kable, E.J.D., 1974. Sea floor basalt alteration: some chemical and Sr isotopic effects. Contributions to Mineralogy and Petrology 44, 219±230.
Haskin, L.A., Haskin, M.A., Frey, F.A., Wildman, T.R., 1968. Relative and absolute terrestrial abundance of the rare earths. In: Ahrens, L.H. (Ed.), Origin and Distribution of the Elements. Pergamon, Oxford, pp. 889±911.
Hein, J., Gibbs, A., Clague, D., Torresan, M., 1996. Hydrothermal mineralization along submarine rift zones Hawaii. Marine Georesources Geotechnology 14 (2), 177±203.
Henin, S., 1956. Synthesis of clay minerals at low temperature. National Conference for Clays and Clay Mineralogy. National Academy of Science±National Research Council Publication, pp. 507±525.
Honnorez, J., 1981. The aging of the oceanic crust at low temperature. In: Emiliani, E. (Ed.), The Sea. Wiley, New York, pp. 525±587.
Kastner, M., Gieskes, J.M., 1976. Interstitial water profiles and sites of diagenetic reactions, Leg 35 DSDP, Bellinghausen abyssal plain. Earth and Planetary Science Letters 33, 11±20.
Laverne, C., Vivier, G., 1983. Petrographical and chemical study of basement basalts from the Galapagos spreading center, Leg 70. Initial Reports Deep Sea Drilling Project 70, 375±389.
Lee, J.H., Byrne, R.H., 1993. Complexation of trivalent rare earth elements (Ce, Eu, Gd, Tb, Yb) by carbonate ions. Geochimica Cosmochimica Acta 57, 295±302.
Ludden, J.N., Thompson, G., 1978. Behaviour of rare earth elements during submarine weathering of tholeiitic basalt. Nature 274, 147±149.
Moore, D.M., Reynolds, R.C.J., 1989. X-Ray Diffraction and the Identification and Analysis of Clay Minerals. Oxford Press, Oxford, 332 pp.
Morgan, J.J., Stumm, W., 1964. Colloid-chemical properties of manganese dioxides. Journal of Colloid Science 9, 347±359.
Nelson, E.P., Forsythe, R.D., 1989. Ridge collision at convergent margins: implications for Archean and post-Archean crustal growth. Tectonophysics 161, 307±315.
Norton, D.R., Papp, C.S.E. (Eds.), 1990. Determination of moisture and total water in silicate rocks. Quality Assurance Manual for the Branch of Geochemistry, U.S. Geol. Surv. Open-File Rep. 90±668, pp. 73±82.
Perkins, W.T., Pearce, N.J.G., Jeffries, T.E., 1993. Laser ablation inductively coupled plasma mass spectrometry: a new technique for the determination of trace elements in silicates. Geochimica et Cosmochimica Acta 57, 475±482.
Pichler, T., 1994. Effects of seawater-rock interaction in a submarine environment: Alteration of basalt from the Southern Chile Ridge. MS Thesis, Colorado School of Mines, Golden, 120 pp.
Ponnamperuma, F.N., Loy, T., Tianco, E.M., 1969. Redox equilibria in flooded soils: II. The manganese oxide systems. Soil Science 108, 48±57.
Ross, C.S., Hendricks, S.B., 1945. Minerals of the montmorillonite group, their origin and relation to soils and clays. U.S.G.S. Professional Paper 205 B, 23±79.
Seyfried, W.R.J., Bischoff, J.L., 1979. Low temperature basalt alteration by seawater: an experimental study at 70°C and 150°C. Geochimica et Cosmochimica Acta 43, 1937±1947.
Seyfried, W.E.J., Shanks, W.C.I., Dibble, W.E.J., 1978. Clay mineral formation in DSDP leg 34 basalt. Earth and Planetary Science Letters 41, 265±276.
Stakes, D.S., Scheidegger, K.F., 1981. Temporal variations in secondary minerals from Nazca Plate basalts. In: Kulm, L.D. (Ed.), Nazca Plate: Crustal Formation and Andean Convergence. Geological Society of America, pp. 109±130.
Staudigel, H., Hart, S.R., 1983. Alteration of basaltic glass: Mechanisms and significance for the oceanic crust-seawater budget. Geochim. Cosmochim. Acta 47, 337±350.
Stokes, K.R., 1971. Further investigation into the nature of the

minerals chlorophaeite and palagonite. Mineral Magazine 38, 205±214.
Stumm, W., Morgan, J.J., 1996. Aquatic Chemistry. Wiley-Interscience, New York, 1022 pp.
Sun, S.S., McDonough, W.F., 1989. Chemical and isotopic systematics of ocean basalts: implications for mantle composition and processes. In: Saunder, A.D., Norry, M.J. (Eds.), Magmatism in the Ocean Basins. Geological Society of London, pp. 313±345.
Taggart, J.E. Jr. et al., 1987. Analysis of geologic materials by wavelength-dispersive X-ray fluorescence spectrometry. U.S. Geological Survey Bulletin 1770, E1±E19.
Taylor, S.R., McLennan, S.M., 1985. The Continental Crust: Its Composition and Evolution. Geoscience Texts. Blackwell Scientific Publications, Oxford, 312 pp.
Thompson, G., 1973. A geochemical study of the low-temperature interaction of sea water and oceanic igneous rocks. EOS Trans. Am. Geophys. Union 54, 1015±1019.
Thompson, G., 1991. Metamorphic and hydrothermal processes: basalt±seawater interactions. In: Floyd, P.A. (Ed.), Oceanic Basalts. Blackie, Glasgow, pp. 148±173.
Weaver, C.E., Pollard, L.D., 1975. The Chemistry of Clay Minerals. Developments in Sedimentology, Vol. 15. Elsevier, Amsterdam, 213 pp.